Synthesis, Structure, and Multiply Enhanced Field-Emission Properties of Branched ZnS Nanotube–In Nanowire Core–Shell Heterostructures

Ujjal K. Gautam,[†,‡,§,*] Xiaosheng Fang,[†,‡,§,*] Yoshio Bando,[†] Jinhua Zhan,[#] and Dmitri Golberg[†,‡]

[†]International Center for Materials Nanoarchitectonics (MANA), World Premier International Research Center and [‡]Nanoscale Materials Center, National Institute for Materials Science (NIMS), Namiki 1-1, Tsukuba, Ibaraki 305-0044, Japan, and [#]Department of Chemistry, Key Laboratory of Colloid & Interface Chemistry, Shandong University, Ministry of Education, Jinan 250100, China. [§]These authors contributed equally to this work.

ABSTRACT We report on the synthesis of a novel core–shell metal-semiconductor heterostructure where In forms the core nanowire and wurtzite ZnS forms the shell nanotube. In addition, controlled reaction conditions result in the growth of secondary quasi-aligned ZnS nanowires as numerous branches on the shell nanotubes. These hierarchical architectures are attractive for two reasons: (i) the sharp and quasi-aligned ZnS tips of the nanostructures are potential field-emitters and (ii) since In in bulk form is superconducting the synthesis of core In nanowires should now pave the way for further investigations on magnetic *versus* transport behavior in type-1 superconductors at the nanoscale. The synthesis could be achieved by employing a rapidly heating carbothermal chemical vapor deposition technique and a high reaction temperature. Transmission electron microscopy reveals that the core In nanowires are single crystals, whereas, within a hierarchical shell, the stem and the branches are separated with a crystalline interface. Field-emission measurements demonstrate remarkably large field enhancement which is explained on the basis of a sequential stepwise enhancement mechanism involving the consecutive stem and branch contributions. The present new nanoarchitectures are envisaged to be an important candidate for potential nanoelectronic devices.

KEYWORDS: core–shell nanostructure · 1D heterostructure · hierarchical structure · aligned nanowire · field emission · growth mechanism

One-dimensional (1D) nano/heterostructures consisting of two important functional materials are essential for developing potential nanoelectronic and optoelectronic devices.[1–17] In particular, core–shell heterostructures consisting of two components with distinct functionality often exhibit enhanced performances, such as emission efficiency[16] and high electron mobility,[17] that are the key factors for many device performances. For example, Lieber and co-workers showed that the Ge/Si core–shell nanowires (NW) are high-performance field-effect transistors due to the reduced interface scattering.[1] Ni nanowires encapsulated within fullerene cables exhibit enhanced and anisotropic ferromagnetic behavior along the nanowire axes.[17] Fabrication of such structures formed through a confined growth of a metal core inside a semiconducting shell is not only important for fundamental studies but also for diverse advanced functional devices, for example, interconnects and emitters, *etc.*

Branched 1D nanostructures constitute a unique class of materials where tiny nanowire branches grow on a larger nanowire stem of same or different functionality. This class of materials has an additional advantage of largely increased surface area. The smaller nanostructures may be stabilized by anchoring them on a larger structure and thus creating the possibility of a multifunctional single-component nanodevice.[3,18–20] For example, branched heterostructures made of ZnO stems and Zn_3P_2 branches exhibit highly efficient spatially resolved photodetector characteristics.[3] Very recently, Jung *et al.* have reported on a sequential seeding technique to obtain branched heterojunction nanowires of different compositions.[20] Since the branched structures have sharp tips and are attached on a long backbone they have an effectively high aspect ratio and hence should harbor excellent field-emission properties, such as those discovered in the cases of ZnO and AlN.[21,22]

Being motivated by a unique possibility to merge two materials with vastly different electronic properties we have investigated the growth of 1D heterostructures composed of a metal and a semiconductor. In this communication, we report on the synthesis of an important core–shell structure wherein In metal forms the cores and ZnS forms the shell nanotubes. We further show that controlled conditions lead to the

*Address correspondence to Gautam.Ujjal@nims.go.jp, Fang.Xiaosheng@nims.go.jp.

Received for review January 9, 2008 and accepted April 01, 2008.

Published online April 29, 2008.
10.1021/nn800013b CCC: $40.75

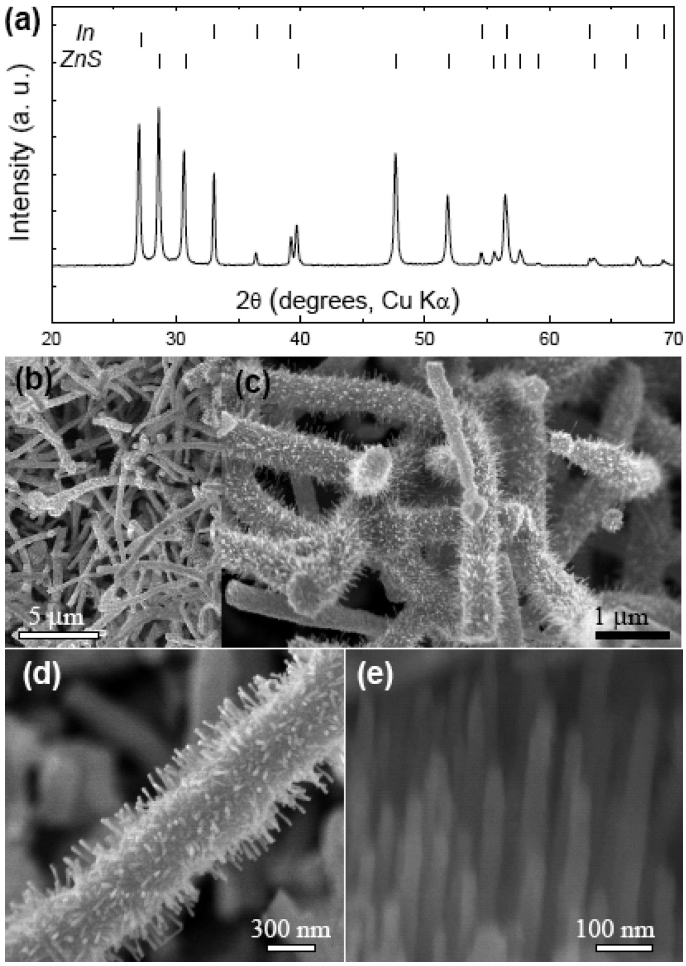

Figure 1. (a) A XRD pattern of the as-prepared heterostructures. The standard peak positions for wurtzite ZnS and In are shown at the panel top. (b, c, d) SEM images of the heterostructures at different magnifications. (e) A high-magnification SEM image showing the ZnS branches quasi-aligned at the heterostructure tip.

secondary growth of ZnS branches on the ZnS mother shells in such a way that the branches are fairly well aligned to each other.

ZnS, a wide bandgap semiconductor with a gap energy of 3.7 eV at 300 K, is one of the first discovered semiconductors which has a wide range of industrial applications.[23,24] Indium is chosen not only because it acts as a catalyst, but also because it is a type-1 superconductor.[25] Indium has a low melting point of 156.7 °C. It has widely been used for making low-melting-point shape-memory alloys.[26] Radioactive ^{111}In is also used for medical imaging of white blood cells.[27] Besides, size-dependent superconducting behavior exhibits quite interesting trends for In nanoparticles[28] and thin films,[29] while the 1D In nanostructures have not been investigated, perhaps because of the synthetic difficulties. Several reports have stated that In can be deposited in the form of nanowire strips on Si substrates[30] and trapped within silica and magnesium oxide nanotubes.[31,32]

The heterostructures reported here have an average length of a few micrometers. The diameter of a core nanowire is ~50−100 nm, whereas a ZnS shell is ~150 nm thick. The branches have a length of ~200 nm and a width of ~20 nm. Considering this interesting morphology, we further investigated its field-emission properties. This shows an unexpected field enhancement. The field-enhancement is normally achieved through two approaches: (i) alignment of the nanostructures, and (ii) increasing their aspect ratios.[33,34] Herein we propose a novel enhancement mechanism wherein both these criteria are addressed.

RESULTS AND DISCUSSION

A wool-like product containing the heterostructures was deposited at the outlet tube placed at the top of graphite chamber inside the furnace. A powder X-ray diffraction (XRD) pattern of a product is displayed in Figure 1a. The pattern clearly indicates a biphase mixture of ZnS (a = 3.82 Å and c = 6.25 Å, JCPDS card: 79−2204) and In (a = 3.25 Å and c = 4.95 Å, JCPDS card: 85−1409). Figure 1b shows a low-magnification scanning electron microscope (SEM) image of the nanostructures. The corresponding high-magnification (HM) SEM images of the product are depicted in Figure 1 panels c and d. The typical lengths of the nanostructures measure from 5 to 20 μm, whereas their diameter varies within 300−800 nm. HMSEM images reveal that 10−20 nm thick and ~100−200 nm long 1D branches decorate the entire nanostructure surface. The branches are oriented at an angle of ~90° with respect to a backbone nanostructure. The branches growing at the tips and middles of a backbone are uniform in dimensions. It is important to note that when zoomed-in these nanorod branches appear to be aligned to each other. In Figure 1d, we present a close view of the quasi-aligned wires.

A transmission electron microscope (TEM) image of a product is displayed in Figure 2a. This shows that the nanostructures have uniform diameter throughout the length. A clear contrast variation at the nanostructure core (Figure 2b) suggests that these 1D structures are composed of two different materials, one forming the core nanowire and the other forming a shell. To investigate the elemental composition throughout the heterostructures, a detailed chemical analysis was carried out using energy dispersive X-ray spectroscopy (EDS). The elemental maps displaced in Figure 2c−f shed the light on the distribution of the constituting elements, that is, Zn, S, In, and C. In Figure 2c,d, the Zn K-edge and the S K-edge signals are evenly distributed throughout the shell structure with a depleting signal at the core. The strong In L-edge signal in the central region (Figure 2e), on the other hand, confirms that

In constitutes the core NW. The corresponding line profiles across the maps are also shown in the insets. Additionally, a thin layer of amorphous carbon creates a coating on the nanostructures (discussed later). Figure 2f is a C K-edge map of the heterostructure.

To understand the structural aspects, detailed analysis was performed using high-resolution (HR) TEM. The branches consist of defect-free single-crystalline ZnS nanorods, as shown in Figure 3 panels a and b. Two growth directions were observed. The lattice fringes in the Figure 3a are separated by a 3.0 Å distance corresponding to the (0002) planes of hexagonal ZnS. The inset shows a nanobeam diffraction pattern taken from a nanorod along the [2−1−10] zone axis. We further confirmed the reciprocal lattice peaks through a 2D-Fourier transform (FFT), Figure 3c. This reveals an exact match with the experimental pattern. Figure 3b illustrates another nanorod branch, with a lattice fringe separation of 3.2 Å. The corresponding FFT and SAED patterns can be indexed to the [0001] zone axis of wurtzite ZnS. Thus, about 70% of the branches grow along the [0001] direction and have an abrupt flat end, whereas the remaining portion grows along the [10−10] direction. The later branches have gradually terminating round tips. It is interesting to note the unusual growth direction along the [10−10] orientation, which was also previously observed by Xiong *et al.*[35] Figure 3e is an EDS spectrum obtained from a single nanobranch. This verifies the branch composition as Zn:S ≈ 1:1. Note that the nanostructures have a thin coating of amorphous carbon (see Supporting Information). Figure 3f presents a stem-branch interface. The investigations of numerous interfaces have shown that no epitaxial relationship exists between the branches and a mother nanotube. In this case, they are inclined at an angle of 22°. The core In NWs are single crystals as inferred from the electron diffraction patterns. Figure 3 panels h and i show two SAED patterns acquired from two segments of the same NW depicted in Figure 3g. The similar orientations in these patterns indicate the unidirectional growth of single-crystalline NWs. Indium has a low melting point and hence, by using a convergent electron beam, it was possible to melt it inside a nanotube. In addition, because of sudden expansion of a confined In core, we observed the explosion-like events through electron irradiation (see Supporting Information).

Diverse functional properties could be expected from these heterostructures. For example, while their magnetic behavior would be attuned to their metallic cores, their optical performance would be largely governed by ZnS shields. The interesting low-temperature magnetic behavior of the In nanowires are being pursued currently and the results will be presented in detail in a separate communication. Among many potential applications, these heterostructures are envisaged to be highly efficient field-emitters owing to their 1D morphology and sharply pointed ZnS tips. Notably, at any given configuration, lying or standing, there would always be sharp and aligned tips pointing toward the anode. This is highly desirable for strong emission. It should be mentioned that until now the studies on the field-emission (FE) properties of ZnS nanostructures have been rather limited compared to other field-emitters such as carbon nanotubes and ZnO nanomaterials.[34] The emission properties of the present heterostructures were studied at various anode-sample separations and within a 100−1100 V bias voltage range. Figure 4a shows a FE current density, *J*, obtained when the anode was placed at a distance of 210 and 150 μm. The measurements reveal a turn-on current density of 10 μA/cm^2 at applied voltages of 5.56 and 5.43 V/μm, respectively. The FE current density can reach 1.1 mA/cm^2 when the applied macroscopic field is 7.45 V/μm.

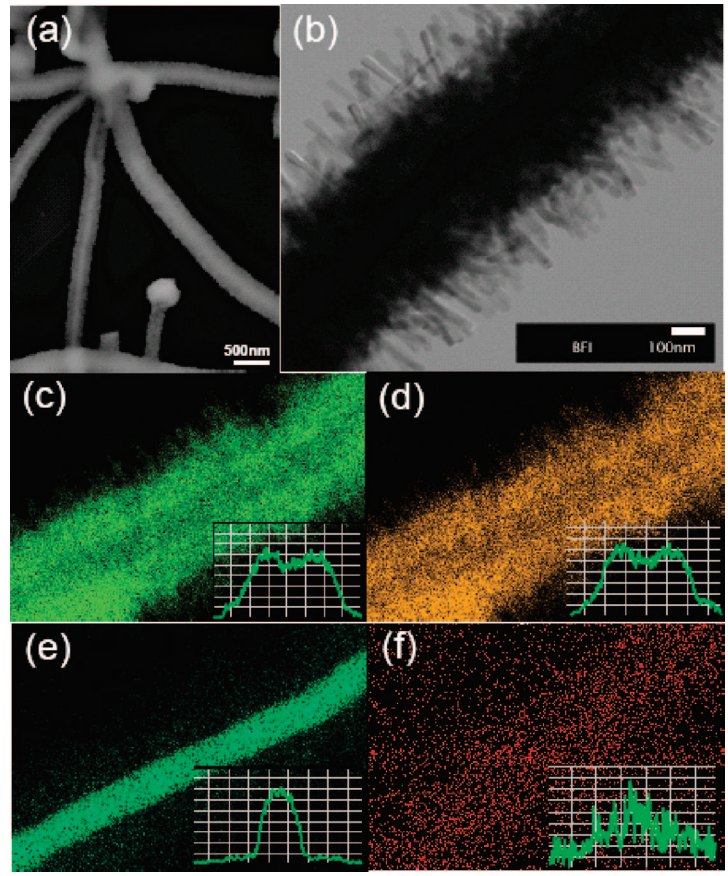

Figure 2. (a) A low-magnification TEM image of the heterostructures; (b) a STEM image of a structure segment. A clear contrast difference between the core and the shell is due to the different scattering from In and ZnS species. EDS maps depict the distribution of the constituting elements within the segment shown in panels c, d, e, and f. The images correspond to the Zn K-edge, S K-edge, In L-edge, and C K-edge signals, respectively. The insets show the EDS line scanning profiles across the maps.

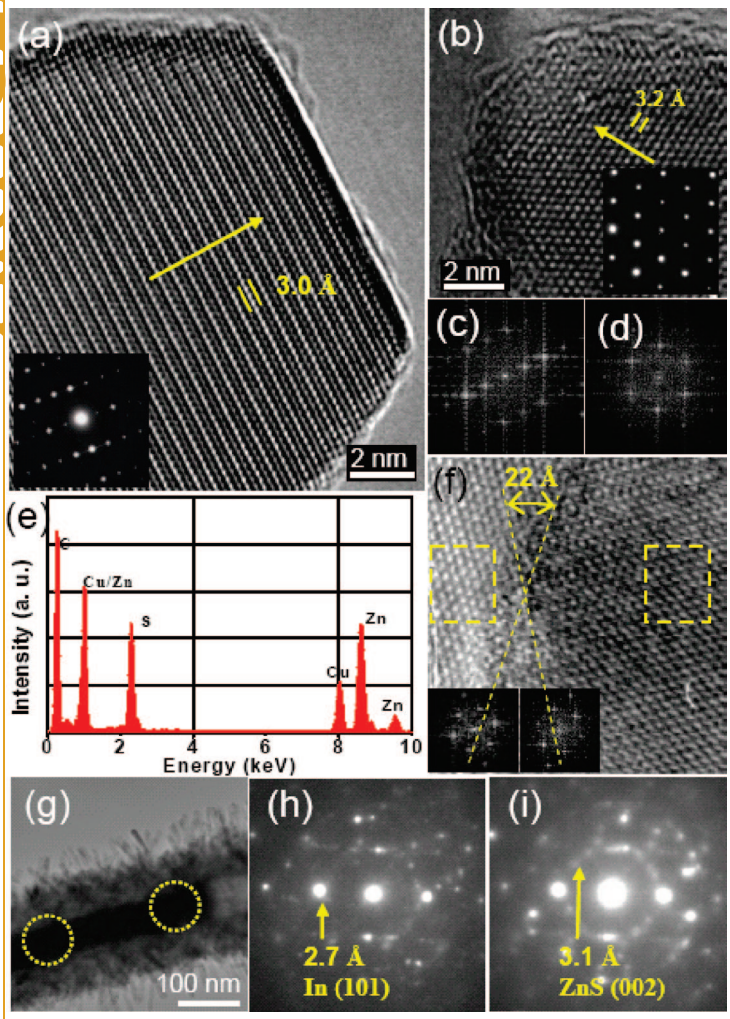

Figure 3. The branches of the heterostructures grown along two different directions of wurtzite ZnS: (a) A HRTEM image of a branch growing along the [0001] axis. The corresponding SAED pattern from its tip is shown in the inset: (b) similar data for a branch growing along the [10−10] direction; (c, d) FFT patterns obtained from the HRTEM images in panels a and b, respectively; (e) EDS pattern acquired from the tip in panel a; (f) HRTEM image of a stem-branch interface. FFT patterns obtained from either sides of the interface are shown in the insets. These indicate an estimated crystal orientation mismatch of 22°; (g) partial In-filling of a ZnS tube; (h, i) SAED patterns taken at different spots on NW. These suggest that the NW is a single crystal.

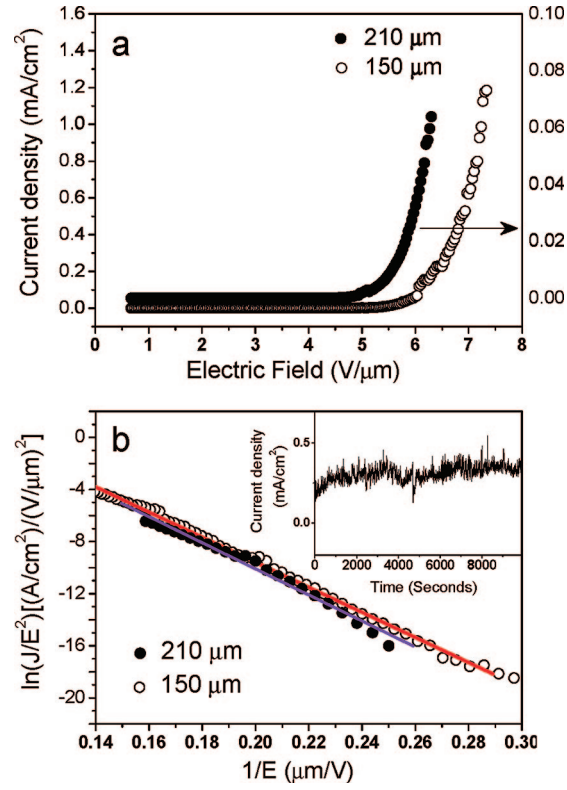

Figure 4. Field-emission properties of the heterostructures. (a) *J*−*E* data obtained at two different anode-sample distances; (b) corresponding Fowler–Nordheim plots. The colored lines are linear fit to the data. The inset in panel b is the field-emission stability data for the heterostructures obtained over ~3 h and acquired at an emission current density of 0.25 mA/cm^2.

Field-emission is a quantum phenomenon where electron tunnels from the cathode to the anode through vacuum upon an applied bias. This can be explained on the basis of the Fowler−Nordheim equation:[34]

$$J = (A\beta^2E^2/\varphi)\exp(-B\varphi^{3/2}/\beta E) \quad (1)$$

or

$$\ln(J/E^2) = \ln(A\beta^2/\varphi) - B\varphi^{3/2}/\beta E \quad (2)$$

where $A = 1.54 \times 10^{-6}$ A eV V^{-2}, $B = 6.83 \times 10^3$ eV$^{-3/2}$ V μm^{-1}, β is the field-enhancement factor, and φ is the work function of the emitting materials, which is 7.0 eV for ZnS.[36] The field-enhancement factor, β, represents the effective field at the emission centers which is dependent on the tip geometry and the aspect ratio of the nanostructures. From eq 2, a plot of ln (J/E^2) *versus* 1/*E* is a straight line, and its slope can be employed to determine β. Thus from Figure 4b, β was found to be 1.6×10^3 at a working anode-sample distance of 210 μm. The field-enhancement and turn-on field values are not only superior to all the previously reported free-standing ZnS nanorods (aspect ratio > 60, β ≈ 400) and nanowires but also rival those of quantum-confined ZnS nanobelts having an extremely high aspect ratios of ~2000.[24,34,37,38]

Stability of the field-emitters is another important parameter related to potential applications. In particular, the nanostructures have small mass, large surface area, and a lower melting point compared to bulk materials of same compositions, making them vulnerable to both chemical and physical damages.[39] A number of external parameters (chemical factors such as surface oxidation, or physical factors such as melting of the emitting centers due to resistive heating) can influence the emission efficiency of a material upon prolonged use. In the inset of Figure 4b, we present a *J*−*T* curve of these heterostructures showing the emission current variations re-

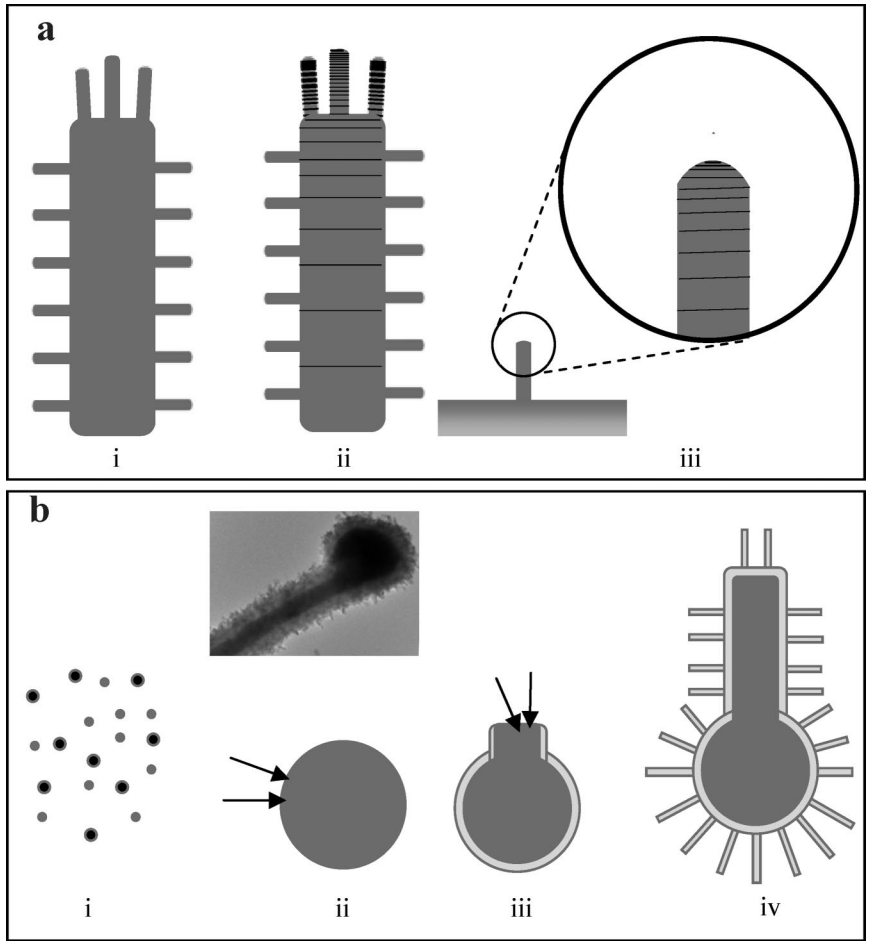

Figure 5. (a) Schematics of field enhancement in a hierarchical nanostructure. The applied field in the first structure is enhanced by a stem first and then by a branch (seen in ii). Thus the effective field experienced by the branch is much larger than in the case of its anchoring on a flat substrate iii. Structure iii also highlights FE contribution from the stem of the nanowires which are lying flat of the substrate. The stems, but for the branches, would have little contribution to the FE properties. (b) Schematics of the growth process: (i) during the initial carbothermal reaction the vapors of Zn, In, CS_2 and S are created; (ii) In forms liquid droplets in which Zn vapor dissolves; (iii) supersaturation leads to precipitation of liquid Zn around the In surface, which reacts with S and CS_2 forming a ZnS shell; (iv) as more vapors are coming and In liquid squeezes out of the nuclei, a ZnS shell grows around the In column. The rapid crystallization of ZnS can create defect sites on the shell structure seeding the ZnS branches growth.

corded over a period of 3 h at a working field of 6.5 V/μm. As seen from the figure, there are not any current degradations or notable fluctuations during this period.

The observed field enhancement is markedly higher than that expected from a simple aspect ratio consideration (~40−50 in this case). The mechanism of field enhancement is suggested to be essentially different in this case because of a hiererchical architecture. The enhancement is expected to replicate a unique structural pattern of an emitter. This can be understood by considering the tip of a single heterostructure vertically facing the anode (Figure 5a). First, the primary applied field would be enhanced by a stem structure which acts as a substrate for the secondary branches. A stronger field at the bottom of the branches is equivalent to an effectively higher applied bias, which then, in turn, is further enhanced by the 1D branches. The case would be entirely different if the branches are anchored onto a flat substrate or if the entire nanostructure has a diameter of the branch. More theoretical work is required to understand these effects quantitatively. In any case, these results open up a new approach for multifold enhancement of FE within a given nanoscale heterostucture. For example, although metals have excellent emission efficiency, it is extremely difficult to obtain their nanostructures at high aspect ratios. The growth of short metal tips made of tungsten, for example, on a 1D substrate could be a smart route toward new efficient emitters.

The growth of present heterostructures is based upon the principles of carbothermal chemical vapor deposition (CVD), as described schematically in Figure 5b. Carbon was used as one of the source materials in this synthesis to reduce the compounds to elements and to produce CS_2 (stage-i).[40,41] Low

melting point In forms large droplets in which Zn slowly dissolves until supersaturation (stage-ii). Further Zn penetration leads to its precipitation across the In droplet surface. The sulfur and CS_2 vapors react with precipitated Zn forming a solid ZnS shell around the In droplet (stage-iii). The inset in Figure 5b displays such a droplet which was observed at each nanostructure end. Owing to the presence of solid and rigid ZnS shell more additions of metal vapor force In liquid to squeeze out of the preformed structure. This results in In column formation. Then the growth process continues around In columns forming the core−shell heterostructures. The control of S vapor supply was found to be crucial during the synthesis. In the absence of an excessive S flow a product contains unreacted Zn and In microcrystals and the heterostructures do not possess branches.

CONCLUSIONS

To conclude, hierarchical core−shell structures consisting of primary ZnS nanotubes, In core nanowires, and ZnS nanowire secondary branches have been created to infuse multifunctionality into a single nanosystem. The synthesis was achieved by high temperature (~1300 °C) carbothermal CVD technique where In acts as a catalyst. This special geometry induces multifold enhanced field-emission. The present nanostructures are expected to become valuable not only in fundamental science but also in device applications.

METHODS

The ZnS−In heterostructures have been synthesized using a high-temperature vertical induction furnace (see Supporting Information).[42] In brief, the furnace consists of a graphite cylinder attached to a gas flowing system at its top and bottom. A copper inductor and a graphite susceptor were used. In a typical synthesis, 0.10 g of In_2S_3, 0.25 g of ZnS, and 0.05 g of activated carbon powder were thoroughly mixed, put into a graphite crucible, and placed at the center of the furnace. A 0.4 g portion of S was placed in another graphite crucible at the furnace bottom where the temperature was estimated to be ~400−500 °C. The furnace was first evacuated to 2×10^{-5} Pa and then filled with 99.99% Ar gas. The crucible was rapidly heated to 1300 °C and maintained at this temperature for 45 min, and then the furnace was switched off allowing the crucible to naturally cool to room temperature. Approximately 0.1g of the product was collected from the deposition tube placed at the top of the crucible. Throughout the reaction, an Ar carrier gas flow was maintained at a rate of 0.2 L/minute. Powder XRD pattern was acquired using a RINT, 2200 diffractometer using Cu X-ray source. Scanning electron microscopy investigation of the sample was carried out using a field emission JEOL JSM-6700F microscope. The heterostructures were dispersed in ethanol by ultrasonication, deposited dropwise onto a holey carbon coated copper grid, and characterized using a high-resolution JEOL JEM-3000F (300 kV) transmission electron microscope. The field-emission properties of the heterostructures were studied at room temperature in a high vacuum chamber (10^{-6} Pa) using a 1 mm^2 cross-sectional area aluminum anode. A dc voltage sweeping from 100 to 1100 V was applied to a sample at a step of 5 V. A dilute dispersion of the nanostructures in toluene was deposited dropwise on a pure Si substrate and vacuum-dried for 48 h.

Acknowledgment. This work was in part supported by World Premier International Research Center Initiative (WPI Initiative) on Materials Nanoarchitronics, MEXT, Japan. X. S. Fang thanks the Japan Society for the Promotion of Science (JSPS) for a support in the form of a fellowship tenable at the National Institute for Materials Science, Tsukuba, Japan. The authors thank Pedro M. F. J. Costa for helpful discussions. J. H. Zhan thanks financial support from NSFC 20501014 and 973 Program 2007CB936602.

Supporting Information Available: Schematic illustration of an induction furnace, a nanostructure with a thicker carbon shell, and in situ TEM images of an explosion-like event occurring in a nanostructure upon its exposure to intense e^- beam. This material is available free of charge *via* the Internet at http://pubs.acs.org.

REFERENCES AND NOTES

1. Lauhon, L. J.; Gudiksen, M. S.; Wang, D.; Lieber, C. M. Epitaxial Core−Shell and Core−Multishell Nanowire Heterostructures. *Nature* **2002**, *420*, 57–61.
2. Rao, C. N. R.; Govindaraj, A. *Nanotubes and Nanowires RSC Nanoscience & Nanotechnology Series*; RSC Publishing: Cambridge, U.K., 2005.
3. Yang, R. S.; Chueh, Y. L.; Morber, J. R.; Snyder, R.; Chou, L. J.; Wang, Z. L. Single-Crystalline Branched Zinc Phosphide Nanostructures: Synthesis, Properties, and Optoelectronic Devices. *Nano Lett.* **2007**, *7*, 269–275.
4. Chueh, Y. L.; Chou, L. J.; Wang, Z. L. SiO_2/Ta_2O_5 Core−Shell Nanowires and Nanotubes. *Angew. Chem., Int. Ed.* **2006**, *45*, 7773–7778.
5. Zhang, D. H.; Liu, Z. Q.; Han, S.; Li, C.; Lei, B.; Stewart, M. P.; Tour, J. M.; Zhou, C. W. Magnetite (Fe_3O_4) Core-shell Nanowires: Synthesis and Magnetoresistance. *Nano Lett.* **2004**, *4*, 2151–2155.
6. Shen, G.; Bando, Y.; Gao, Y.; Golberg, D. Synthesis and Interface Structures of Zinc Sulfide Sheathed Zinc-Cadmium Nanowire Heterojunctions. *J. Phys. Chem. B* **2006**, *110*, 1423–1427.
7. Wu, Y. Y.; Fan, R.; Yang, P. D. Block-by-Block Growth of Single-Crystalline Si/SiGe Superlattice Nanowires. *Nano Lett.* **2002**, *2*, 83–86.
8. Zhan, J. H.; Bando, Y.; Hu, J. Q.; Liu, Z. W.; Yin, L. W.; Golberg, D. Fabrication of Metal-Semiconductor Nanowire Heterojunctions. *Angew. Chem., Int. Ed.* **2005**, *44*, 2140–2144.
9. Gudiksen, M. S.; Lauhon, L. J.; Wang, J.; Smith, D. C.; Lieber, C. M. Growth of Nanowire Superlattice Structures for Nanoscale Photonics and Electronics. *Nature* **2002**, *415*, 617–620.
10. Xia, Y.; Yang, P.; Sun, Y.; Wu, Y.; Mayers, B.; Gates, B.; Yin, Y.; Kim, F.; Yan, H. One-Dimensional Nanostructures: Synthesis, Characterization, and Applications. *Adv. Mater.* **2003**, *15*, 353–389.
11. Rao, C. N. R.; Deepak, F. L.; Gundiah, G.; Govindaraj, A. Inorganic Nanowires. *Prog. Solid State Chem.* **2003**, *31*, 5–147.
12. Bjork, M. T.; Ohlsson, B. J.; Sass, T.; Persson, A. I.; Thelander, C.; Magnusson, M. H.; Deppert, K.; Wallenberg, L. R.; Samuelson, L. One-Dimensional Steeplechase for Electrons Realized. *Nano Lett.* **2002**, *2*, 87–89.
13. Tenne, R. Inorganic Nanotubes and Fullerene-like Nanoparticles. *Nat. Nanotechnol.* **2006**, *1*, 103–111.
14. Li, Y.; Meng, G. W.; Zhang, L. D.; Phillipp, F. Ordered Semiconductor ZnO Nanowire Arrays and Their Photoluminescence Properties. *Appl. Phys. Lett.* **2000**, *76*, 2011–2013.

15. Hu, J. Q.; Bando, Y.; Zhan, J. H.; Golberg, D. Fabrication of Silica-Shielded Ga-ZnS Metal Semiconductor Nanowire Heterojunctions. *Adv. Mater.* **2005**, *17*, 1964–1969.
16. Nirmal, M.; Brus, L. Luminescence Photophysics in Semiconductor Nanocrystals. *Acc. Chem. Res.* **1999**, *32*, 407–414.
17. Tao, F.; Liang, Y.; Yin, G.; Xu, D.; Jiang, Z.; Li, H.; Han, M.; Song, Y.; Xie, Z.; Xue, Z.; Zhu, J.; Xu, Z.; Zheng, L.; Wei, X.; Ni, Y. Concentric Sub-micrometer-Sized Cables Composed of Ni Nanowires and Sub-micrometer-Sized Fullerene Tubes. *Adv. Funct. Mater.* **2007**, *17*, 1124–1130.
18. Li, Y.; Xiang, J.; Qian, F.; Gradecak, S.; Wu, Y.; Yan, H.; Blom, D. A.; Lieber, C. M. Dopant-Free GaN/AlN/AlGaN Radial Nanowire Heterostructures as High Electron Mobility Transistors. *Nano Lett.* **2006**, *6*, 1468–1973.
19. Xu, L.; Su, Y.; Li, S.; Chen, Y.; Zhou, Q.; Yin, S.; Feng, Y. Self-Assembly and Hierarchical Organization of Ga_2O_3/In_2O_3 Nanostructures. *J. Phys. Chem. B* **2006**, *111*, 760–766.
20. Jung, Y.; Ko, D. K.; Agarwal, R. Synthesis and Structural Characterization of Single-Crystalline Branched Nanowire Heterostructures. *Nano Lett.* **2007**, *7*, 264–268.
21. Banerjee, D.; Jo, S. H.; Ren, Z. F. Enhanced Field Emission of ZnO Nanowires. *Adv. Mater.* **2004**, *16*, 2028–2032.
22. Yin, L. W.; Bando, Y.; Zhu, Y. C.; Li, M. S.; Li, Y. B.; Golberg, D. Growth and Field Emission of Hierarchical Single-Crystalline Wurtzite AIN Nanoarchitectures. *Adv. Mater.* **2005**, *17*, 110–114.
23. Moore, D.; Wang, Z. L. Growth of Anisotropic One-dimensional ZnS Nanostructures. *J. Mater. Chem.* **2006**, *16*, 3898–3905.
24. Fang, X. S.; Zhang, L. D. One-dimensional (1D) ZnS Nanomaterials and Nanostructures. *J. Mater. Sci. Technol.* **2006**, *22*, 721–736.
25. Richards, P. L.; Tinkham, M. Far-Infrared Energy Gap Measurements in Bulk Superconducting In, Sn, Hg, Ta, V, Pb, and Nb. *Phys. Rev.* **1960**, *119*, 575–590.
26. Ishikawa, H.; Sutou, Y.; Omori, T.; Oikawa, K.; Ishida, K.; Yoshikawa, A.; Umetsu, R. Y.; Kainuma, R. Pd-In-Fe Shape Memory Alloy. *Appl. Phys. Lett.* **2007**, *90*, 261906.
27. Nowak, B.; Weber, C.; Schober, A.; Zeiffer, U.; Liehn, E. A.; Von-Hundelshausen, P.; Reinartz, P.; Schaefer, W. M.; Buell, U. Indium-111 Xine Labelling Affects the Cellular Integrity of Haematopoietic Progenitor Cells. *Eur. J. Nucl. Med. Mol. Imaging* **2007**, *34*, 715–721.
28. Wu, F. Y.; Yang, C. C.; Wu, C. M.; Wang, C. W.; Li, W. H. Superconductivity in Zero-Dimensional Indium Nanoparticles. *J. Appl. Phys.* **2007**, *101*, 09G111.
29. Okuma, S.; Nishida, N. Disappearance of Superconductivity and Critical Resistance in Thin Indium Films. *Physica C* **1991**, *185*, 1925–1926.
30. Fleischer, K.; Chandola1, S.; Esser, N.; McGilp, J. F. Optical Properties of Indium Nanowires-an Adsorption Study. *Phys. Stat. Sol. B* **2005**, *242*, 2655–2663.
31. Golberg, D.; Li, Y. B.; Mitome, M.; Bando, Y. Real-Time Observation of Liquid Indium Unusual Behavior Inside Silica Nanotubes. *Chem. Phys. Lett.* **2005**, *409*, 75–80.
32. Tang, C. C.; Bourgeois, L.; Bando, Y.; Golberg, D. Preparation and Structure of Magnesium Oxide Coated Indium Nanowires. *Chem. Phys. Lett.* **2003**, *382*, 374–380.
33. Fan, S. S.; Chapline, M. G.; Franklin, N. R.; Tombler, T. W.; Cassell, A. M.; Dai, H. J. Self-Oriented Regular Arrays of Carbon Nanotubes and Their Field Emission Properties. *Science* **1999**, *283*, 512–514.
34. Fang, X. S.; Bando, Y.; Gautam, U. K.; Ye, C. H.; Golberg, D. Inorganic Semiconductor Nanostructures and Their Field-Emission Applications. *J. Mater. Chem.* **2008**, *18*, 509–522.
35. Xiong, Q.; Chen, G.; Acord, J. D.; Liu, X.; Zengel, J. J.; Gutierrez, H. R.; Redwing, J. M.; Voon, L. C. L. Y.; Lassen, B.; Eklund, P. C. . Optical Properties of Rectangular Cross-sectional ZnS Nanowires. *Nano Lett.* **2004**, *4*, 1663–1668.
36. Ruyven, L. J.; Williams, F. E. Valence-band Bending to Fermi Level and Radiative Recombination in ZnS With Liquid Electrodes. *Phys. Rev. Lett.* **1966**, *16*, 889–890.
37. Chang, Y. Q.; Wang, M. W.; Chen, X. H.; Ni, S. L.; Qiang, Q. J. Field Emission and Photoluminescence Characteristics of ZnS Nanowires *via* Vapor Phase Growth. *Solid State Commun.* **2007**, *142*, 295–298.
38. Ghosh, P. K.; Maiti, U. N.; Jana, S.; Chattopadhyay, K. K. Field Emission from ZnS Nanorods Synthesized by Radio Frequency Magnetron Sputtering Technique. *Appl. Surf. Sci.* **2006**, *253*, 1544–1550.
39. Wei, W.; Liu, Y.; Wei., Y.; Jiang, K. L.; Peng, L. M.; Fan, S. S. Tip Cooling Effect and Failure Mechanism of Field-Emitting Carbon Nanotubes. *Nano Lett.* **2007**, *7*, 64–68.
40. Zhu, Y. C.; Bando, Y.; Xue, D. F.; Golberg, D. Nanocable-Aligned ZnS Tetrapod Nanocrystals. *J. Am. Chem. Soc.* **2003**, *125*, 16196–16197.
41. Rao, C. N. R.; Gundiah, G.; Deepak, F. L.; Govindaraj, A.; Cheetham, A. K. Carbon-Assisted Synthesis of Inorganic Nanowires. *J. Mater. Chem.* **2004**, *14*, 440–450.
42. Gautam, U. K.; Bando, Y.; Zhan, J.; Costa, P. M. F. J.; Fang, X. S.; Golberg, D. Ga-doped ZnS Nanowires-Precursors for $ZnO/ZnGa_2O_4$ Nanotubes. *Adv. Mater.* **2008**, *20*, 810–814.